COBEM 2023 27TH INTERNATIONAL CONGRESS OF MECHANICAL ENGENEERING

ABCM Brazilian Society of Mechanical Sciences and Engineering
27th ABCM International Congress of Mechanical Engineering
December 04-08, 2023, Florianópolis-SC, Brazil

COB-2023-1458
NUMERICAL STUDY OF THE INFLUENCE OF THE DISTANCE BETWEEN THE INLET BOUNDARY CONDITION AND THE OBSTACLE IN EXTERNAL FLOW

Cleberson da Silva Matos
José Emanuel da Silva Montiel
Valentina Ferro Antunes de Oliveira
Escola Politécnica da Universidade de São Paulo – Departamento de Engenharia de Construção Civil
cleberson.matos@usp.br, jose.montiel@usp.br, valentina.ferro@usp.br

Laís Corrêa
Universidade Federal da Grande Dourados – Faculdade de Ciências Exatas e Tecnologia
laiscorrea@ufgd.edu.br

Fernando Akira Kurokawa
Escola Politécnica da Universidade de São Paulo – Departamento de Engenharia de Construção Civil
fernando.kurokawa@usp.br

Abstract. *Computational Fluid Dynamics (CFD) has been widely employed to study and analyze the behavior of fluids in physical systems. Studies on mesh convergence have been necessary for validation and application of models, as well as for replication of experimental cases. When dealing with external flows, the inappropriate positioning of the inlet boundary condition can provide inaccurate numerical results, causing significant changes in the velocity field and drag coefficient of a simulation. An insufficiently large distance could cause a disturbance at the inlet and alter the results, while an unnecessarily large distance would increase the computational cost of the simulation. In this context, this work aims to contribute to the topic by means of a numerical analysis of the influence of the distance between the inlet boundary condition and the object, verifying the existence of interferences through analysis of the velocity field and the drag coefficient. To do so, a cylinder with a diameter of 1 m was taken as a basis, which has numerical and experimental results available in the literature. The methods used consist of modeling a mesh capable of producing results that agree with the available literature data, varying the distance between the inlet and the object thereafter. For each simulation performed, the velocity field, drag coefficient, lift coefficient and pressure coefficient were obtained and subsequently compared. The computational simulations developed and presented in this work were carried out with the aid of the CFD software OpenFOAM, using LES (Large-Eddy Simulation) Smagorinsky turbulence model. The results obtained indicated that from a certain distance onward, the variation of the velocity field became significantly reduced, suggesting that the coefficients started to converge to a specific value. The methodology presented in this work can be applied using other CFD methods, so that the results will be useful for later applications.*

Keywords: *Computational Fluid Dynamics, Inlet distance, Mesh conversion, Velocity field, Drag coefficient.*

1. INTRODUCTION

Computational Fluid Dynamics (CFD) is the art of replacing the integrals or the partial derivates in equations with discretize algebraic forms, which in turn are solved to obtain numbers for the flow field values at discrete points in time and/or space (Anderson, 2017). It employs mathematical algorithms and computational techniques to simulate and predict fluid behavior, providing valuable insights into complex fluid dynamics problems (Versteeg & Malalasekera, 2007). By solving the governing equations of fluid motion, such as the Navier-Stokes equations, CFD enables the visualization and analysis of flow patterns, pressure distributions, velocity profiles, and other important fluid properties (Ferziger & Peric, 2013). This versatile tool finds applications in various industries, including aerospace, automotive, energy, and environmental engineering, assisting in the design, optimization, and performance evaluation of diverse engineering systems (Hirsch, 2007).

In particular, the accuracy of numerical simulations in Computational Fluid Dynamics (CFD) relies heavily on the implementation of appropriate modeling and validation techniques, including mesh convergence studies (Anderson, 2017) (Versteeg & Malalasekera, 2007) and careful consideration of boundary conditions (Ferziger & Peric, 2013). Mesh convergence studies involve refining the computational grid to achieve a balance between computational efficiency and accuracy, ensuring that the solution is independent of the grid resolution (Roache, 1998). Additionally, accurately

capturing the behavior of fluid flow requires careful consideration of boundary conditions, which define the inflow, outflow, and wall conditions of the domain being simulated (Patankar, 1980).

In the context of external flows, the positioning of the inlet boundary condition plays a crucial role in obtaining reliable numerical results (Löhner, 2008). The accurate placement of the inlet boundary condition is essential as it directly influences the behavior of the flow field near the object of interest. An inappropriate positioning of the inlet boundary condition can lead to distorted velocity profiles, incorrect pressure distributions, and inaccurate predictions of flow characteristics. To ensure the fidelity of the numerical simulations, careful consideration must be given to the location and orientation of the inlet boundary condition, taking into account the desired flow regime and the specific characteristics of the external flow problem (Ferziger & Peric, 2013).

Recent works (Malveira, 2018), (Prsic, et al., 2016) and (Zhang, et al., 2016) do not clearly explain the criterion used for positioning the distance of the inlet boundary condition from the obstacle; they only mention the distance used and indicate that the mesh is adequate by through a convergence study. The first work used 5.5 obstacle sizes, the second work used 10 obstacle sizes, and the third work does not mention the distance used. Similarly, (Li, et al., 2017) used 10 obstacle sizes and stated that the distance is sufficient to eliminate the far-field effects from the flow upstream of the cylinders.

Conversely, an older paper (Wanderley & Levi, 2000) does not cite the criterion for the position the distance of the inlet boundary condition from the obstacle, but only uses 20 cylinder diameters. Since the choice is not motivated by a specific criterion, the question remains as to what distance should be used in the simulations.

In his paper, Nigam (Nigam, 2018) talks about how to place inlet and outlet boundary conditions in CFD simulations, looking at the effects of the proximity of the inlet and outlet boundaries for interior and exterior flows of an incompressible fluid. The analytical results obtained for external flows, indicate that we would have to locate the exterior boundaries of the computational domain at a distance on the order of 100 obstacle sizes in 2D and 10 obstacle sizes in 3D.

Because of this, the objective of this study is to enhance our understanding of the influence of the distance between the inlet boundary condition and the object in external flow simulations. Given the significance of this factor in the accuracy of numerical predictions, this research aims to contribute to the existing knowledge by conducting a comprehensive numerical analysis. By systematically varying the distance between the inlet boundary condition and the object, the study will investigate the resulting changes in the flow behavior, such as velocity field patterns and drag coefficients. Through these analyses, valuable insights can be gained, providing guidance for optimal placement of the inlet boundary condition and improving the reliability of external flow simulations.

To investigate the influence of the distance between the inlet boundary condition and the obstacle in external flow, a well-established test case is chosen. A cylinder with a known diameter of 1 m is selected for this purpose, as it has been extensively studied and documented in the literature, providing reliable numerical and experimental results. By utilizing this test case, it becomes possible to compare and validate the numerical simulations against existing data, ensuring the accuracy and credibility of the study's findings.

2. NUMERICAL METHODOLOGY

2.1 Governing equations

The Large-Eddy Simulation (LES) model has the ability to model moderately high Reynolds number flows and capture the three-dimensional characteristics of bluff body flows in a computationally efficient manner compared to Direct Numerical Simulation (DNS). In an LES model, the large-scale turbulence is directly simulated, while the subgrid-scale turbulence, which is considered to be more independent of specific cases, is modeled (Prsic, et al., 2013).

This present study involves conducting numerical simulations to solve the three-dimensional unsteady and incompressible governing equations of fluids. The continuity and Navier-Stokes equations, modified for three-dimensional LES using the Sub-Grid Scale (SGS) model, are presented in Eq. (1) and Eq. (2).

$$\frac{\partial \overline{u_i}}{\partial x_i} = 0, \tag{1}$$

$$\frac{\partial \overline{u_i}}{\partial t} + \overline{u_j}\frac{\partial \overline{u_i}}{\partial x_j} = -\frac{1}{\rho}\frac{\partial \bar{p}}{\partial x_j} + \frac{\partial}{\partial x_i}([\nu + \nu_{SGS}]\frac{\partial \overline{u_i}}{\partial x_j}), \tag{2}$$

Where u_i is velocity in i th direction; x_i is displacement in i th direction; t is time; ρ is density; p is pressure; ν is kinematic viscosity; ν_{SGS} is the sub-grid scale viscosity; and the overbar represents filtered, grid-scale (GS) components.

Filtering is accomplished by performing spatial averaging on the Navier-Stokes equations through a convolution operation using the spatial filter G(r), as in Eq. (3) (Pope, 2000):

$$\overline{u_x} = \int_{-\infty}^{\infty} u_x(x-r)G(r)dr, \tag{3}$$

The filter function G(r) is implemented as a basic box filter with a width equivalent to the cubic root of the cell volume, which corresponds to the cell size in the uniform hexahedral mesh employed ($r = \Delta x$). This partitioning of the flow distinguishes the grid-scale (GS) and sub-grid scale (SGS) components (Blackmore, et al., 2013). The filtering process introduces residual stresses, which are modeled using the Boussinesq approximation by incorporating an SGS eddy viscosity based on the Smagorinsky model, as in Eq. (4) and (5) (Smagorinsky, 1963):

$$\nu_{SGS} = (C_s \Delta_g)^2 + \sqrt{2\overline{S_{ij} S_{ij}}}, \tag{4}$$

$$S_{ij} = \frac{1}{2}\left[\frac{\partial u_i}{\partial x_j} + \frac{\partial u_j}{\partial x_i}\right], \tag{5}$$

Where C_s is the Smagorisnky coefficient and Δ_g is the grid size.

The simulations are conducted using the OpenFOAM®, utilizing the PISO (Pressure Implicit with Splitting of Operators) algorithm to solve the Navier-Stokes equations (Ferziger & Peric, 2001).

2.2 Domain and boundary condition

In this paper, external flow of a viscous fluid on a circular section prism is studied, according to the literature (Braun, 2002), obtaining as a result the velocity fields and drag coefficients measured over the analysis time. The case was studied for Reynolds number (Re) $Re = 10^3$.

The Figure 1 illustrates the geometric characteristics of the problem and the boundary conditions. At the inlet, a velocity (U) was imposed, while a homogeneous Neumann boundary condition applied for the pressure. At the cylinder surface, the no-slip condition was used. At the top and bottom surfaces, the symmetry condition was applied. Finally, at the outlet surface, a homogeneous Neumann condition was imposed for velocity, while for pressure, a static pressure of zero was used. These conditions are shown in the Table 1.

In the computational framework, the convective term was handled using the QUICK (Quadratic Upstream Interpolation for Convective Kinematics) numerical scheme. To account for temporal variations, the Crank-Nicolson numerical scheme was implemented. Additionally, the Laplacian term was treated using the Gauss linear numerical scheme.

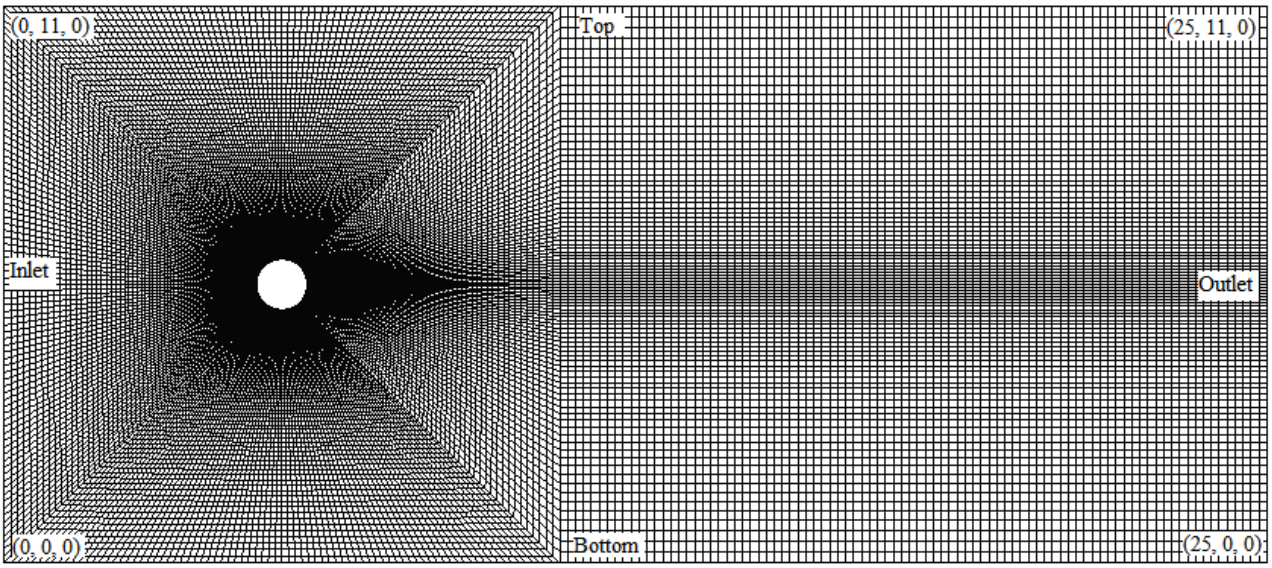

Figure 1. Geometric characteristics.
(*) Coordinates for the center of the cylinder: (5.5,5.5,0).
(*) Coordinates in meters.

Table 2 presented the parameters employed for the simulations in this work.

Table 1. Boundary condition.

Location	Boundary condition
Inlet flow	velocity-inlet, $U = 10\ m/s$
Outlet	patch
Top and Bottom	symmetryPlane
Front and Back	empty
Cylinder	wall

Table 2. Physical and geometrical constants.

Parameter	Value
Kinematic viscosity (ν)	$0.01\ m^2/s$
Velocity inlet – U	$10\ m/s$
Characteristic size – D (Diameter)	1.0 m
Time	30 s
Time step[(1)]	1.8×10^{-4} s

[(1)] The time step was set to keep the Courant number below 1.

2.3 Grid independence study

In order to determine an appropriate mesh for the simulation, a grid independence study was conducted, employing five different mesh densities: Mesh A (63,847 nodes), Mesh B (111,502 nodes), Mesh C (195,800 nodes), Mesh D (261,096 nodes), and Mesh E (111,506 nodes). The Mesh E exhibited superior refinement near the object and reduced refinement as we moved away, aiming to optimize computational costs without compromising accuracy. The Figure 2 shows the near-wall region in the meshes A and E.

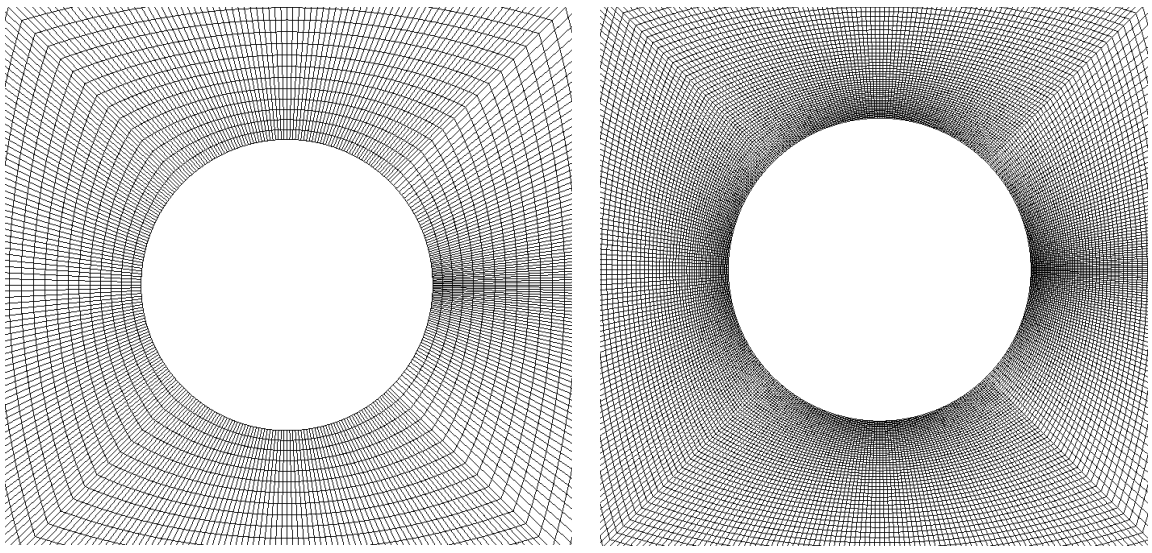

(a) Mesh A (b) Mesh E

Figure 2. Detail of the mesh A and E.

The drag coefficient (C_d) was used as the parameter to assess the convergence of the simulation results, with the reference value obtained from Braun (Braun, 2002) as 1.62. The results of the grid independence study are presented in Table 3, where the statistical convergence criterion, the relative error, was used for the average value of C_d in an interval of 20 to 30 s (this interval was chosen because the flow is in a permanent regime) with the reference value.

When comparing the results with the reference, the Mesh E obtained satisfactory results, with a percentage deviation of 0.17%. Therefore, considering the precision of the results and the reduced computational cost, this mesh will be used to verify the position of the inlet boundary condition.

Table 3. Grid independence study.

Mesh	Nodes	Elements	C_d	Relative error (%)
Mesh A	63847	31510	1.6767	3.50
Mesh B	111502	55260	1.6592	2.42
Mesh C	195800	97224	1.6565	2.25
Mesh D	261096	129760	1.6397	1.22
Mesh E	111506	55240	1.6228	0.17

3. METHODOLOGY

The methodology employed in this study involves systematically varying the distance from the inlet boundary condition to the cylinder. By adopting this approach, the drag coefficients and velocity fields are computed for each distinct distance. This allows a comprehensive examination of the influence of the distance on the resulting flow characteristics.

A total of ten simulation cases were conducted in this study, encompassing a range of distances between the inlet boundary condition and the object, hereafter denoted by d_{inlet}. The specific configurations for each case, including the corresponding distances, node quantities, and element quantities, are summarized in Table 4.

Table 4. Simulation cases.

Simulation	d_{inlet} (m)	Nodes	Elements
CASE 1	5.5	111506	55240
CASE 2	6.5	116260	179729
CASE 3	7.5	117250	181244
CASE 4	8.5	118240	182759
CASE 5	9.5	119230	184274
CASE 6	10.0	120220	185789
CASE 7	11.5	121210	187304
CASE 8	12.0	122200	188819
CASE 9	20.0	132100	203969
CASE 10	100.0	200410	308504

Specifically, Figure 3 demonstrates the mesh modification applied when the distance between the inlet and the object was established at 10 m. The mesh was carefully designed to uphold its refinement, ensuring the absence of deformations in both the mesh and the flow dynamics near the object. The parameters and boundary conditions remained consistent with those used in the grid independence study.

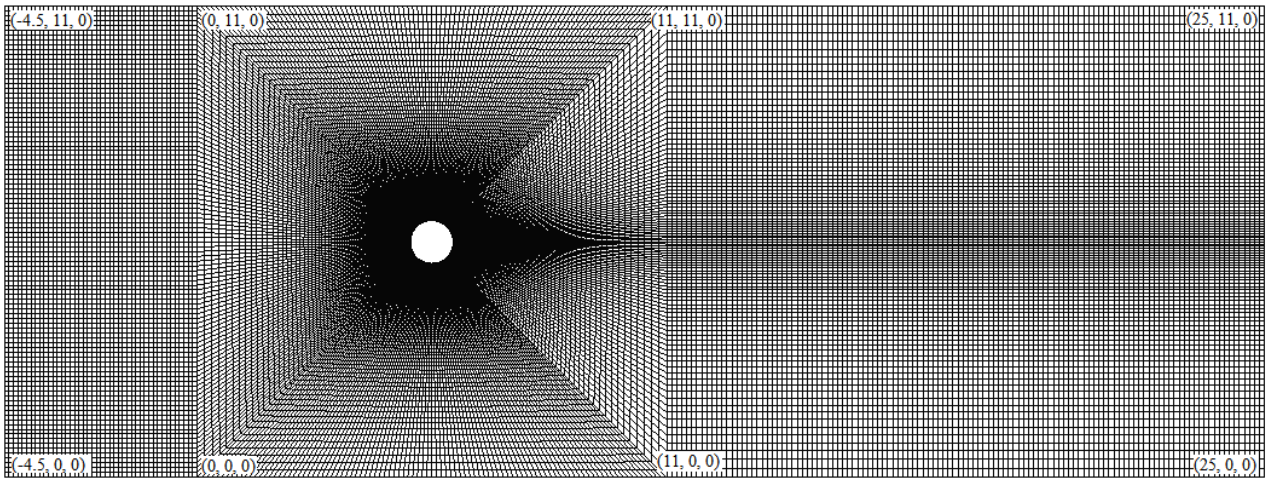

Figure 3. Coordinates of the modified mesh.
(*) Coordinates for the center of the cylinder: (5.5,5.5,0).
(*) Coordinates in meters.

4. RESULTS AND DISCUSSIONS

This section presents a comprehensive analysis of the numerical simulations performed to investigate the influence of the distance between the inlet boundary condition and the cylinder on its aerodynamic coefficients.

Figure 4 and Figure 5 shows the velocity and pressure fields extracted for the final simulation time (t = 30 s). It is possible to see the stagnation point, the maximum pressure point and the Kármán vortex street, an expected phenomenon for this type of flow.

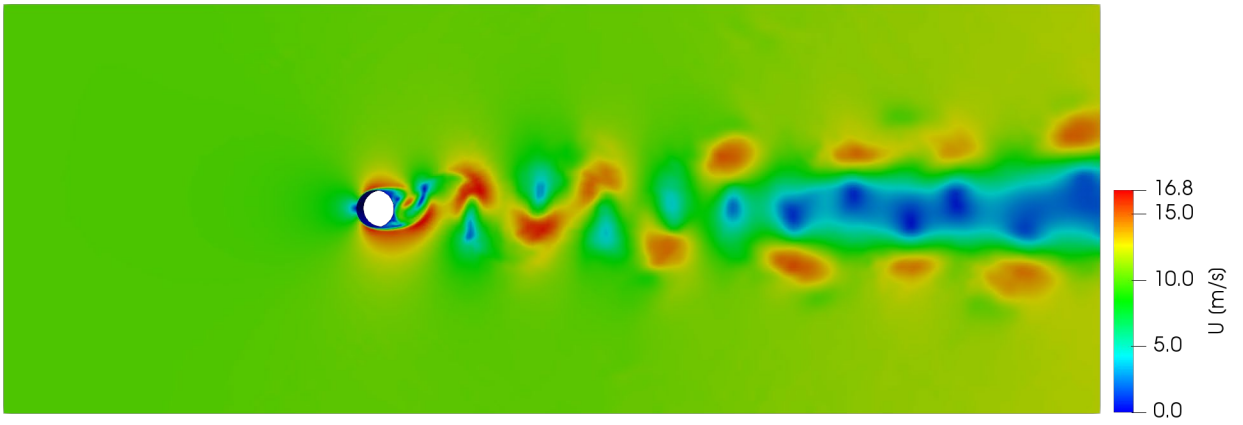

Figure 4. Velocity field for the case 6 at time = 30 s.

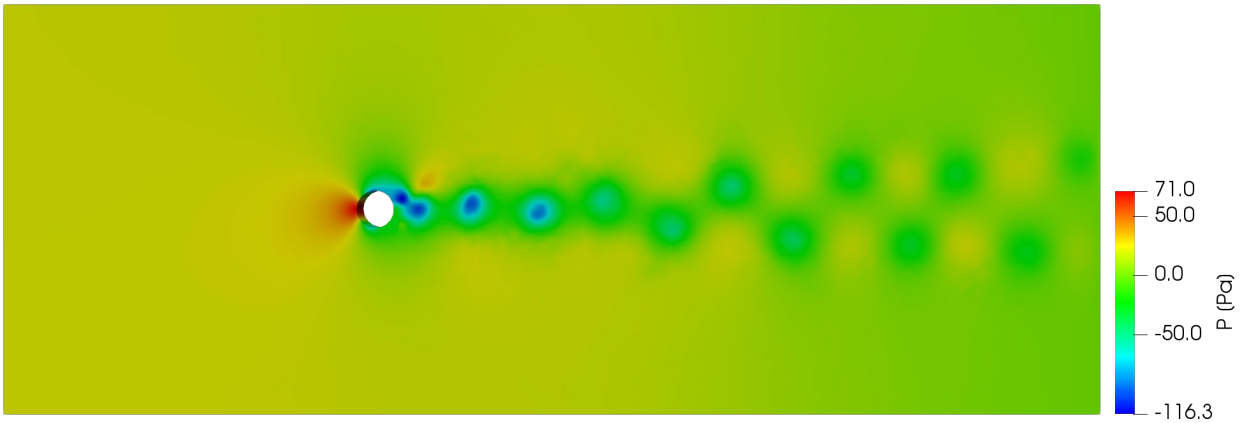

Figure 5. Pressure field for the case 6 at time = 30 s.

For a precise understanding of the velocity field variation, Figure 6 shows the horizontal component of velocity field variation extracted from the horizontal plane corresponding to the center of the cylinder (center line in relation to the vertical axis of the mesh). The d_{inlet} axis starts from the cylinder with coordinates (0.5, 5.5, 0) and goes to the beginning of each tested domain. The velocity values were extracted at different distances from the cylinder, but for better visualization only the cases 1, 2, 3, 6 and 10 were plotted.

As can be seen, the velocity starts at 10 m/s and goes to zero at the stagnation point. However, for the case with the smallest d_{inlet}, case 1, this velocity has a certain upward displacement, which means that for the same distance it has higher values when compared to the other cases. For the other cases, the velocity graph practically overlaps, which indicates that even the difference in d_{inlet} between them no longer affects the horizontal velocity.

Table 5 and Table 6 exhibits the results of the drag coefficient (C_d) and the lift coefficient (C_l) for the interval of 20 to 30 s (this interval was chosen because the flow is in a permanent regime), where C_d is given by the average value while C_l is calculated from the root mean square (rms). The relative error between each case and the previous one was used as statistical convergence criterion to determine whether there was convergence towards a specific value.

It can be seen that there is a decrease in C_d from case 1 to case 3, followed by a stabilized value, with a maximum variation of 0.09% from case 8 to case 9. A similar behavior its observable in C_l, where there is a maximum deviation of 0.5% between cases 6 and 7, after the value has stabilized. This may indicate that for a $d_{inlet} \geq 7.5$ m (used in case 3), the values of the coefficients can be considered constant, showing a very small influence of d_{inlet}.

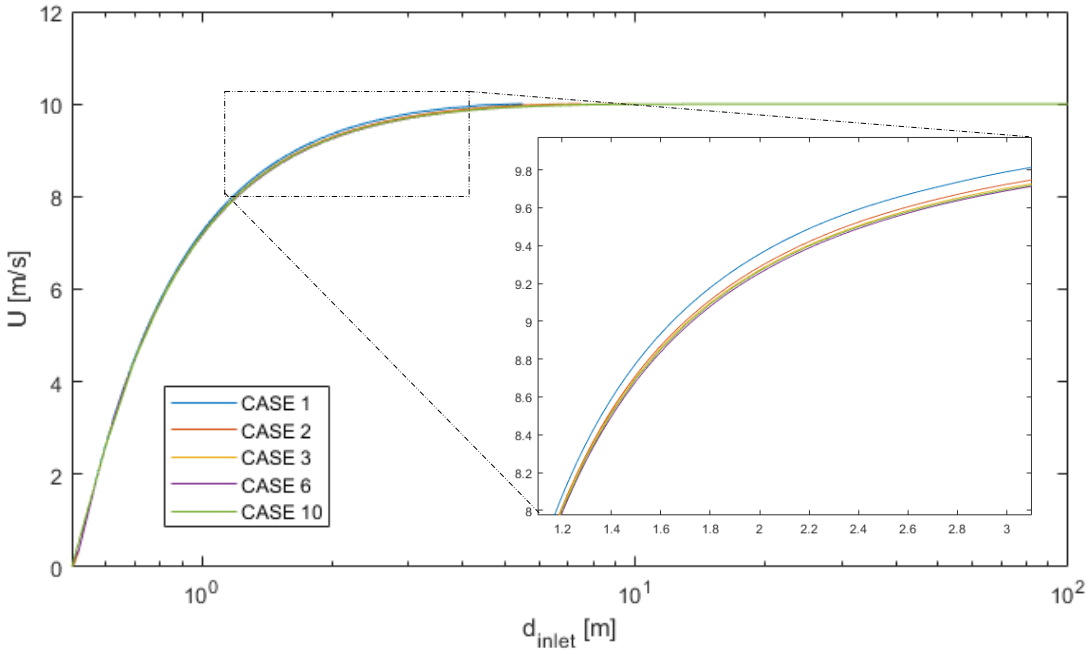

Figure 6. Velocity field variation.

Table 5. Results of the C_d for the simulation cases.

Simulation	d_{inlet} (m)	C_d	Relative error with the previous case (%)
CASE 1	5.5	1.6228	-
CASE 2	6.5	1.6005	1.37
CASE 3	7.5	1.5856	0.93
CASE 4	8.5	1.5844	0.08
CASE 5	9.5	1.5849	0.03
CASE 6	10.0	1.5850	0.01
CASE 7	11.5	1.5845	0.03
CASE 8	12.0	1.5832	0.08
CASE 9	20.0	1.5818	0.09
CASE 10	100.0	1.5812	0.04

Table 6. Results of the C_l rms for the simulation cases.

Simulation	d_{inlet} (m)	C_l rms	Relative error with the previous case (%)
CASE 1	5.5	1.1309	-
CASE 2	6.5	1.1029	2.48
CASE 3	7.5	1.0840	1.71
CASE 4	8.5	1.0868	0.26
CASE 5	9.5	1.0884	0.15
CASE 6	10.0	1.0907	0.21
CASE 7	11.5	1.0853	0.50
CASE 8	12.0	1.0846	0.06
CASE 9	20.0	1.0847	0.01
CASE 10	100.0	1.0851	0.04

Figure 7 illustrates the behavior of drag and lift coefficients for the cases with the largest relative error and for stabilization, during the entire simulation time. It can be observed that case 1 shows the greatest variation compared to the other cases plotted.

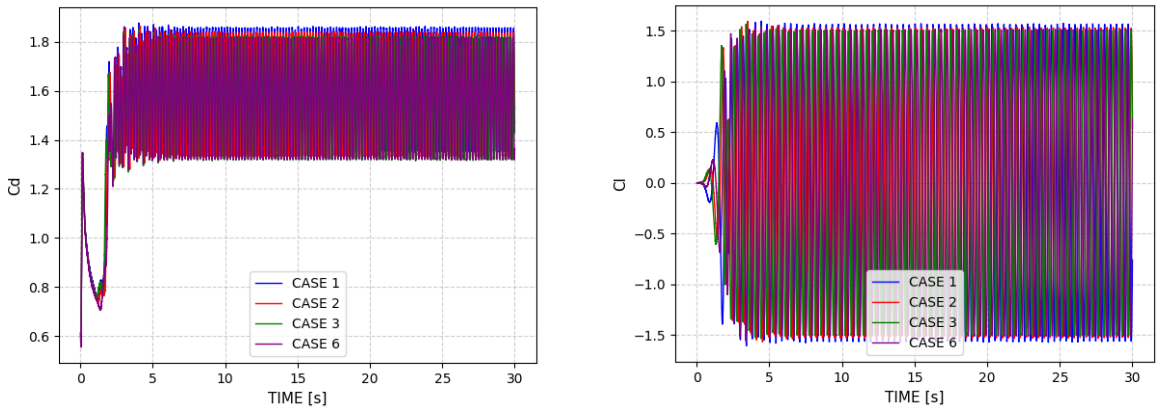

Figure 7. Drag (C_d) and Lift (C_l) coefficients.

As another way of verifying this difference, Figure 8 shows the average pressure coefficient (C_p) that was plotted in an interval of 20 to 30 s. Similarly, case 1 demonstrates the most significant deviation when compared to the other plotted cases. For the other cases, its observable the stabilization of the coefficient value.

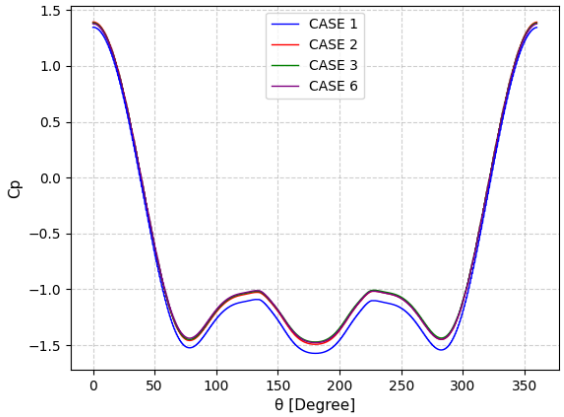

Figure 8. Pressure coefficient (C_p).

5. CONCLUSIONS

In conclusion, this study successfully investigated the influence of the distance between the inlet boundary condition and the object on external flow behavior through numerical simulations. By systematically varying the distances and carefully tuning the computational mesh, valuable insights into the flow dynamics and pressure distributions near the obstacle were obtained. The results obtained provided a clear understanding that the 7.5 m of the cylinder make the difference for the coefficients below 1%. It was found that the drag, lift and pressure coefficients stabilize at this distance.

Despite the limitations of the shape, the results of this study offer significant contributions to the field of Computational Fluid Dynamics (CFD) and external flow simulations. By elucidating the impact of the distance between the inlet boundary condition and the object, this work provides essential guidance for accurately positioning the inlet boundary condition in a 2D cylinder case, further studies should be carried out on other shapes.

6. ACKNOWLEDGEMENTS

Support for this research was provided by the Brazilian agencies, CNPq (Conselho Nacional de Desenvolvimento Científico) and FAPESP (Fundação de Amparo à Pesquisa do Estado de São Paulo), Grants 2022/01072-4.

7. REFERENCES

Anderson, J. D., 2017. *Computational Fluid Dynamics: The Basics with Applications.*. New York: McGraw-Hill Education.

Blackmore, T., Batten, W. M. & Bahaj, A. S., 2013. Inlet grid-generated turbulence for large-eddy simulations. *International Journal of Computational Fluid Dynamics*, 11 September, pp. 307-315.

Braun, A. L., 2002. *Um modelo para a simulação numérica para a ação do vento sobre seções de pontes.* Porto Alegre: Univerisdade Federal do Rio Grande do Sul.

Ferziger, J. H. & Peric, M., 2013. *Computational Methods for Fluid Dynamics.* 3ª ed. Berlin: Springer.

Ferziger, J. & Peric, M., 2001. *Computational Methods for Fluid Dynamics Methods for Fluid Dynamics.* Berlin, Germany: Springer-Verlag.

Hirsch, C., 2007. *Numerical Computation of Internal and External Flows: The Fundamentals of Computational Fluid Dynamics.* 2ª ed. Amsterdam: Elsevier.

Li, Z., Prsic, M. A., Ong, M. C. & Khoo, B. C., 2017. Large Eddy Simulations of flow around two circular cylinders in tandem in the vicinity of a plane wall at small gap ratios. *Journal of Fluids and Structures*, 12 October, pp. 251-271.

Löhner, R., 2008. *Applied CFD Techniques: An Introduction Based on Finite Element Methods.* 2ª ed. Chichester: John Wiley & Sons.

Malveira, L. F. C., 2018. *Investigação numérica de modelos de turbulência no escoamento do vento em pontes suspensas.* São Paulo: Master's Thesis.

Nigam, M., 2018. *How to Place Inlet and Outlet Boundary Conditions in CFD Simulations.* [Online] Available at: https://www.comsol.com/blogs/how-to-place-inlet-and-outlet-boundary-conditions-in-cfd-simulations/ [Acesso em 01 June 2023].

Patankar, S. V., 1980. *Numerical Heat Transfer and Fluid Flow.* 1ª ed. Washington: Taylor & Francis.

Pope, S., 2000. *Turbulent Flows.* Cambridge: Cambridge University Press.

Prsic, M. A., Ong, M. C., Pettersen, B. & Myrhaug, D., 2013. Large Eddy Simulations of flow around a smooth circular cylinder in a uniform current in the subcritical flow regime. *Ocean Engineering*, 15 December, pp. 61-73.

Prsic, M. A., Ong, M. C., Pettersen, B. & Myrhaug, D., 2016. Large Eddy Simulations of flow around a circular cylinder close to a flat seabed. *Marine Structures*, 30 January, pp. 127-148.

Roache, P. J., 1998. *Verification and Validation in Computational Science and Engineering.* New York: Hermosa Publishers.

Smagorinsky, J., 1963. GENERAL CIRCULATION EXPERIMENTS WITH THE PRIMITIVE EQUATIONS. *Montly Weather*, 1 March, pp. 99-164.

Versteeg, H. K. & Malalasekera, W., 2007. *An Introduction to Computational Fluid Dynamics: The Finite Volume Method.* 2ª ed. Harlow: Pearson Education Limited.

Wanderley, J. & Levi, C., 2000. Validation of a finite difference method for the simulation of vortex-induced vibrations on a circular cylinder. *Ocean Engineering*, 15 August, pp. 445-460.

Zhang, K. et al., 2016. Numerical study on the effect of shape modification to the flow around circular cylinders. *Journal of Wind Engineering and Industrial Aerodynamics*, 28 February, pp. 23-40.

8. RESPONSIBILITY NOTICE

The authors are the only responsible for the printed material included in this paper.